A Shell Model for Real-Time Medical Simulation

Olivier Comas, Stéphane Cotin and Christian Duriez

INRIA, Alcove team, Lille, France

Abstract. Contributions: Shell model with real-time implementation + method for fitting medical data

1 Introduction

1.1 Related work

Numerous models are available in the literature to describe physics of thin objects, from fairly simple and naive approaches to more complex and thorough representations. Continuum mechanics provides many formulations able to accurately describe stresses occurring within thin objects. Most of them fall into one of the following two categories: plate theory or shell theory. Those theories have been a subject of interest in the mechanical community for decades. The difference between these two kinds of structures is very well explained by Liu *et al.* [1] and can be summarized by the fact that plate bending elements can only carry transversal loads while shells can undergo more complex deformations. For instance, if we consider the horizontal board of a bookshelf, that board can be approximated as a plate structure and the transversal loads are the weight of the books. A typical deformation of the board is illustrated in figure 1 left. Conversely, a shell structure can carry loads in all directions, and therefore can undergo bending, twisting and in-plane deformation (see Figure 1 right). Considering the folded shape of the implant within the injection device (see Figure **??**), a thin plate model would not correctly capture the deformation and therefore a shell formulation was retained to model the intra-ocular lens behaviour.

Development of a satisfactory physical model that runs in real-time but produces visually convincing animation of thin objects has been a challenge in Computer Graphics, particularly in the area of cloth modelling. Rather than resorting to shell theory which involves the most complex formulations in continuum mechanics, previous works have often relied on discrete formulations. Early approaches to cloth modelling only considered in-plane deformation, and often relied on mass-spring models (see [2], [3] or [4] for instance). More recent works have considered adding bending through angular springs. For instance Taskiran *et al.* [5] have chosen to use a linear representation of angular springs to supply bending and torsion effects in hair modelling, which allowed them to simulate curly hair with good realism. Wang *et al.* [6] successfully used a network of linear and angular springs to describe bending and twisting of catheters and guidewires in an interventional radiology simulator. Yet, such models are

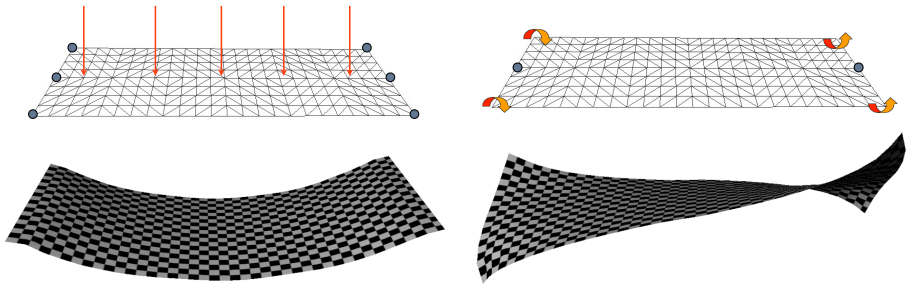

Fig. 1. Illustration of a key difference between various models of thin objects. While thin plate theory allows to describe bending (left), it cannot represent more complex deformations such as twist (right) which is captured by shell theory.

limited in their ability to describe certain behaviour, as they do not rely on continuum mechanics. Another limitation of such models is the difficulty to derive spring stiffness (in particular for angular springs) from elastic properties (Young's modulus and Poisson's ratio). For these reasons, other approaches have been proposed. Among the different models introduced recently we can mention the work of Choi *et al.* [7] and Bridson *et al* [8]. Choi *et al.* proposed a real-time simulation technique for thin shells undergoing large deformations. The authors adopt the energy functions from the discrete shells proposed by [9]. For real-time integration of the governing equation, they adapted a modal analysis technique, called modal warping. The resulting simulations run in real-time even for large meshes, and the model can handle large bending and/or twisting deformations with acceptable realism. Bridson *et al.* followed the same energy approach to derive their bending model but improved the resolution of the equations by suggesting a novel mixed implicit/explicit integration scheme. They also presented a post-processing method for treating cloth-character collisions that preserves folds and wrinkles. Pabst *et al.* improved the bending modelling used by Bridson *et al.* to allow the integration of measured material data. A method to use thin shell dynamics with point sampled surfaces for efficient animation was recently proposed by Wicke *et al.* [10] where the curvature of the shell is measured through the use of fibers.

In this paper we consider the problem of lens implant folding, unfolding and deployment within a very constrained space. An important difference with previous works is that the ratio stiffness / mass of artificial lenses is very high compared to many material (such as fabric), resulting in added difficulties to obtain a numerically stable simulation. Indeed, if the mass density of cotton and acrylic is about the same, the stiffness of intra-ocular implants is three orders of magnitude higher. The closest work to what we propose is the one of Thomaszewski *et al.* [11] who derive their formulation from thin shell analysis in

a co-rotational framework. However, the authors use very soft and deformable material (Young's modulus $E = 5000\,Pa$ and Poisson's ratio $\nu = 0.25$).

2 Co-rotational triangular shell model

We propose to define a triangular shell element by combining a two-dimensional in-plane membrane energy, with an off-plane energy for describing bending and twist (see figure 2). To allow for real-time simulation, a computationally efficient formulation is needed. We therefore propose to extend the co-rotational idea introduced by Fellippa in [12]. Indeed co-rotational approaches have been successfully applied to real-time simulation of volumetric objects over the last few years [13]. They offer a good trade-off between computational efficiency and accuracy by allowing small deformations but large displacements. We propose to improve and extend a plate model first introduced by Przemieniecki [14] to a co-rotational formulation. Once combined with an in-plane membrane formulation we obtain an accurate, yet computationally efficient, shell finite element method featuring both membrane and bending energies.

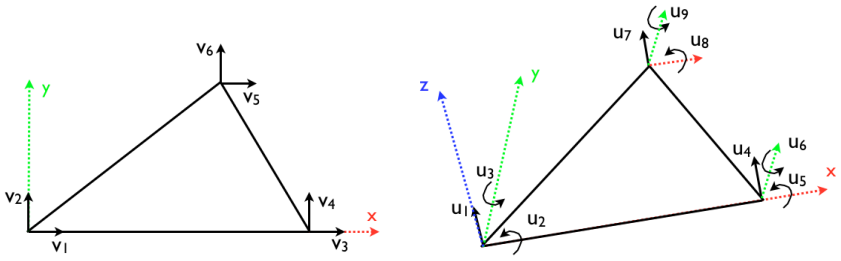

Fig. 2. A triangular shell element can be defined as a combination of a triangular in-plane membrane element (left) and a triangular thin plate in bending (right). The different degrees of freedom v and u of both models are illustrated above.

2.1 Triangular elastic membrane

The computation of the triangular elastic membrane stiffness matrix can be derived from previous works dealing with tetrahedral co-rotational elements (see Muller *et al.* [13] for instance). The element stiffness matrix $\mathbf{K}_e$ can be computed as follows:

$$\mathbf{K}_e = \int_v \mathbf{J}\boldsymbol{\chi}\mathbf{J}^T dV \tag{1}$$

where $\mathbf{J}$ is the strain-displacement matrix and $\boldsymbol{\chi}$ embodies the material's behaviour. The implant is very stiff and we therefore assume that the local

deformations remain limited during the deployment and a linear constitutive law is sufficient. Thus in the simple case of Hooke's law we have:

$$\boldsymbol{\chi} = \frac{E}{12(1-\nu^2)} \begin{bmatrix} 1 & \nu & 0 \\ \nu & 1 & 0 \\ 0 & 0 & \frac{1}{2}(1-\nu) \end{bmatrix} \tag{2}$$

The stiffness matrix in the global frame is eventually obtained using the rotation matrix of the element: $\mathbf{K} = \mathbf{R}\mathbf{K}_e\mathbf{R}^T$ where $\mathbf{R}$ describes the rotation of the (triangular) element with respect to its initial configuration.

2.2 Triangular plate bending

To calculate the stiffness matrix for the transverse deflections and rotations shown on figure 2, we start with the assumed deflection u_z of the form

$$u_z = c_1 + c_2x + c_3y + c_4x^2 + c_5xy + c_6y^2 + c_7x^3 + c_8xy^2 + c_9y^3 \tag{3}$$

where $c_1, \ldots, c_9$ are constants. Equation 3 solves an issue of symmetry which was observed with the deflection function proposed by Przemieniecki in [14]. These constants can be evaluated in terms of the displacements and slopes at the three corners of the triangular plate using

$$\mathbf{u} = \mathbf{C}\mathbf{c} \tag{4}$$

where $\mathbf{u} = \{u_1 u_2 \ldots u_9\}$ and $\mathbf{c} = \{c_1 c_2 \ldots c_9\}$. Matrix $\mathbf{C}$ derives from equation 4:

$$C = \begin{bmatrix} 1 & 0 & 0 & 0 & 0 & 0 & 0 & 0 & 0 \\ 0 & 0 & 1 & 0 & 0 & 0 & 0 & 0 & 0 \\ 0 & -1 & 0 & 0 & 0 & 0 & 0 & 0 & 0 \\ 1 & x_2 & 0 & x_2^2 & 0 & 0 & x_2^3 & 0 & 0 \\ 0 & 0 & 1 & 0 & x_2 & 0 & 0 & 0 & 0 \\ 0 & -1 & 0 & -2x_2 & 0 & 0 & -3x_2 & 0 & 0 \\ 1 & x_3 & y_3 & x_3^2 & x_3y_3 & y_3^2 & x_3^2 & x_3y_3^2 & y_3^3 \\ 0 & 0 & 1 & 0 & x_3 & 2y_3 & 0 & 2x_3y_3 & 3y_3^2 \\ 0 & -1 & 0 & -2x_3 & -y_3 & 0 & -3x_3^2 & -y_3^2 & 0 \end{bmatrix} \tag{5}$$

The notations

$$u_1 = (u_z)_{x_1,y_1} \qquad u_2 = \left(\frac{\partial u_z}{\partial y}\right)_{x_1,y_1} \qquad u_3 = -\left(\frac{\partial u_z}{\partial x}\right)_{x_1,y_1} \tag{6}$$

and so on for the two other vertices, were used.

We can calculate the strains from the flat-plate theory using:

$$e_{xx} = -z\frac{\partial^2 u_z}{\partial x^2} \tag{7}$$

$$e_{yy} = -z\frac{\partial^2 u_z}{\partial y^2} \tag{8}$$

$$e_{xy} = -2z\frac{\partial^2 u_z}{\partial x \partial y} \tag{9}$$

Hence, using the above equations and equation (3), we have

$$\begin{bmatrix} e_{xx} \\ e_{yy} \\ e_{xy} \end{bmatrix} = -z \begin{bmatrix} 0\,0\,0\,2\,0\,0\,6x & 0 & 0 \\ 0\,0\,0\,0\,0\,2 & 0 & 2x\,6y \\ 0\,0\,0\,0\,2\,0 & 0 & 4y & 0 \end{bmatrix} \mathbf{c} \tag{10}$$

or symbolically $\mathbf{e} = \mathbf{D}\mathbf{c}$ where $\mathbf{D}$ stands for the 3×9 matrix in equation 10, including the pre-multiplying constant $-z$. Noting from equation (4) that $\mathbf{c} = \mathbf{C}^{-1}\mathbf{u}$, we have:

$$\mathbf{e} = \mathbf{D}\mathbf{C}^{-1}\mathbf{u} = \mathbf{b}\mathbf{u} \tag{11}$$

where $\mathbf{b} = \mathbf{D}\mathbf{C}^{-1}$. Knowing that the stiffness matrix $\mathbf{K}_e$ for an element is obtained from

$$\mathbf{K}_e = \int_v \mathbf{b}^T \boldsymbol{\chi} \mathbf{b} dV \tag{12}$$

where $\boldsymbol{\chi}$ is the material matrix, the substitution of $\mathbf{b}$ into this expression yields

$$\mathbf{K}_e = (\mathbf{C}^{-1})^T \int_v \mathbf{D}^T \boldsymbol{\chi} \mathbf{D} dV \mathbf{C}^{-1} \tag{13}$$

The integration is carried out numerically using Gauss points located at the middle of each edge of the triangle.

2.3 Implementation

In practical terms, the different computations associated with each triangular shell element can be described as follows:

1. Compute the rotation matrix $\mathbf{R}$ from global to triangle (local) frame
2. Compute the local displacement vector $\mathbf{u} = \{v_1, v_2, 0, u_2, u_3, v_3, v_4, 0, u_5, u_6, v_5, v_6, 0, u_8, u_9\}$ for each of the 3 nodes of the triangle (the nodes have 6 degrees-of-freedom). As we are in a co-rotational framework the normal displacements u_1, u_4, u_7 of all 3 nodes are null in the local frame of the triangle.
3. Compute matrix $\mathbf{D}_i$ at each Gauss point i
4. The strain-displacement matrix at each Gauss point i is computed with $\mathbf{J}_i = \mathbf{D}_i\mathbf{C}^{-1}$
5. Compute the local stiffness matrix $\mathbf{K}_e$ of the element as $\mathbf{K}_e = \sum_{i=1}^{3} \mathbf{J}_i \boldsymbol{\chi} \mathbf{J}_i^T$
6. Transform the local element stiffness matrix into the global frame and add it to a global stiffness matrix

The co-rotational shell formulation has been successfully implemented into the open-source framework SOFA [15].

2.4 Validation

We compared our model with some theoretical results reported by Zhongnian [16] to assess its quality in modelling bending. The test that we carried out uses a square shape mesh clamped on all four edges. A uniform load is then applied on the square and the maximum deflection z_{max} at the centre can be calculated. Several simulations are performed with increasing load values q (ranging from 1 to $5N/m^2$) and the following parameters were used: Young's Modulus $E = 1.092 \times 10^6\, Pa$, Poisson's ratio $\nu = 0.3$, square edge length $L = 10\, m$, thickness $h = 0.1\, m$. Using these particular values it can be shown that $z_{max} = 0.126\, q$. The maximum deflection obtained in our simulations are reported in table 1. In average we found $z_{max} = 0.1248\, q$, resulting in a 0.93 % error between our model and theoretical results on that test.

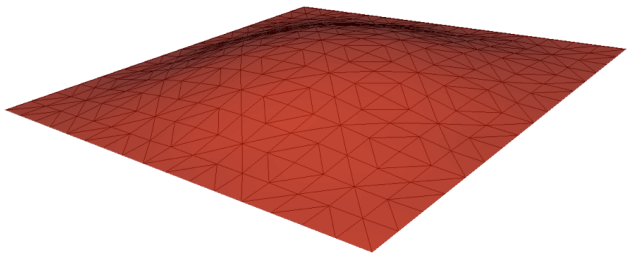

q	z_{max}
1	0.1218
2	0.2475
3	0.3747
4	0.5050
5	0.6374

Table 1. Comparison of our shell model with theoretical results on the bending of a square plate. An error of less than 1 % was found between our simulation and theoretical results.

3 Conclusion

We proposed a co-rotational formulation for shell elements by extending a classical in-plane triangular finite element approach. This simple shell element can efficiently handle both membrane, bending and twist forces. The validity of our approach has been demonstrated though comparison with theoretical results. It was then applied it to a rather complex application: the simulation of intra-ocular lens implant deployment in a cataract surgery simulation. These preliminary results are very encouraging and show the potential of such models. Examples include the modelling of hollow anatomical structures (stomach, colon, etc.), the simulation of cardiac valve leaflets, and blood vessels. Regarding improvements of our current model and simulation, we plan to account for the interaction with the viscoelastic fluid (currently approximated by a high damping). Computation times also need to be improved through the use of more optimised meshes and by porting our parallelisable algorithm to Graphics Processing Units.

References

1. Liu, G., Quek, S.: Finite Element Method: A Practical Course. Butterworth (2003)
2. Provot, X.: Deformation constraints in a mass-spring model to describe rigid cloth behavior. In: Graphics Interface '95. (1995) 147–154
3. Hammer, P.E., Perrinb, D.P., del Nidob, P.J., Howe, R.D.: Image-based mass-spring model of mitral valve closure for surgical planning. In: Proc. of SPIE Medical Imaging. Volume 6918. (2008)
4. Yu, H., Geng, Z.: An improved mass-spring model to simulate draping cloth. IEEE International Conference on Intelligent Computation Technology and Automation **1** (2008) 568–571
5. Taskiran, H.D., Güdükbay, U.: Physically-based simulation of hair strips in real-time. In: WSCG (Short Papers). (2005) 153–156
6. Wang, F., Duratti, L., Samur, E., Spaelter, U., Bleuler, H.: A Computer-Based Real-Time Simulation of Interventional Radiology. In: The 29th Annual International Conference of the IEEE Engineering in Medicine and Biology Society (IEEE-EMBS). (2007) 1742–1745
7. Choi, M.G., Woo, S.Y., Ko, H.S.: Real-time simulation of thin shells. In: ACM SIGGRAPH/Eurographics symposium on Computer animation. (2007) 349–354
8. Bridson, R., Marino, S., Fedkiw, R.: Simulation of clothing with folds and wrinkles. In: Symposium on Computer Animation. (2003) 28–36
9. Grinspun, E., Hirani, A.N., Desbrun, M., Schröder, P.: Discrete shells. In: Proceedings of the Symposium on Computer Animation. (2003) 62–67
10. Wicke, M., Steinemann, D., Gross, M.: Efficient animation of point-sampled thin shells. In: Computer Graphics Forum (Eurographics 2005). Volume 24. (2005) 667–676
11. Thomaszewski, B., Wacker, M., Strasser, W.: A consistent bending model for cloth simulation with corotational subdivision finite elements. In: ACM SIGGRAPH/Eurographics Symposium on Computer Animation. (2006) 107–116
12. Felippa, C.A.: A systematic approach to the element independent corotational dynamics of finite elements. Technical Report CU-CAS-00-03, Center for Aerospace Structures (2000)
13. Muller, M., Gross, M.: Interactive virtual materials. In: Proceedings of Graphics Interface (GI 2004). (2004) 239–246
14. Przemieniecki, J.: Theory of matrix structural analysis. McGraw-Hill (1985)
15. Allard, J., Cotin, S., Faure, F., Bensoussan, P.J., Poyer, F., Duriez, C., Delingette, H., Grisoni, L.: Sofa - an open source framework for medical simulation. In: Medicine Meets Virtual Reality. (2007) 13–18
16. Zhongnian, X.: A simple and efficient triangular fem for plate bending. Acta Mechanica Sinica **2**(2) (1986) 185–192